Published in *Catalysis Today 179 (2012) 102– 114*
doi:10.1016/j.cattod.2011.08.049

Towards the control of intercrystalline mesoporosity in inorganic microporous materials: the case of CoAPO-5

Alicia Manjón-Sanz, Manuel Sánchez-Sánchez* and Enrique Sastre

Instituto de Catálisis y Petroleoquímica, CSIC, C/ Marie Curie, 2
28049 Madrid, Spain

*To whom correspondence should be addressed:
Manuel Sánchez-Sánchez
Telephone number: +34-915854795
Fax number: +34-915854760
E-mail address: manuel.sanchez@icp.csic.es

Abstract

The generation of mesoporosity in microporous materials has been postulated as a valid strategy to limit the diffusional problems of organic substrates within the pores of these materials, without affecting their intrinsic catalytic behavior. This article shows the effect of systematic variations of different synthesis parameters on the nature of the intercrystalline mesoporosity in CoAPO-5 materials. The hard impositions of this approach, including a structure-directing agent (SDA) possessing enough structural specificity towards AFI materials under a very wide range of synthesis conditions, and at the same time having the ability of generating intercrystalline mesoporosity, severely reduces the possible choices. Fortunately, N-methyldicyclohexylamine (MCHA) simultaneously obeys both conditions. We have examined some parameters conventionally affecting the crystallization process such as

time, temperature and dilution, and some other parameters with particular effect on the results of the crystallization of microporous materials such as heteroatom content, heteroatom source, pH of the starting gel and heating source (conventional or assisted by microwave radiation). Excepting Co source, the rest of parameters did have a significant influence on the nature and/or magnitude of intracrystalline mesoporosity. The effect of pH and dilution were particularly relevant, so that ordered intracrystalline mesoporosity is favored when CoAPO-5 is crystallized from relatively diluted and acidic gels. In addition, high Co content produce a higher and better defined mesoporosity, although it implies a modification of the catalytic activity as the number of active centers is inherently varied. Finally, a relevant improvement in the mesoporosity is obtained when heating is assisted by microwave radiation, since the resultant CoAPO-5 is composed by smaller crystals efficiently and orderly agglomerated in pseudospherical particles with a well-defined mesoporosity of narrower pores.

Keywords: Intercrystalline mesoporosity, diffusion, CoAPO-5, N-Methyldicyclohexylamine, MCHA, microwave-assisted synthesis, crystal size, crystal agglomerates, crystal aggregates, hysteresis loop, pH, PSD, pore size distribution

1. Introduction

Microporous materials with pure inorganic frameworks (that is, zeolites and zeotypes) have been widely investigated during the last few decades due to their unique properties [1,2]. Thus, in the field of catalysis, these materials are particularly attractive because of their high thermal and hydrothermal stability and their porous crystalline structure, which confers to them a high surface area and an almost complete exposure of their active sites to organic molecules to be potentially processed. Moreover, their microporous nature offers additional and key catalytic advantages in comparison to those non-porous materials also having high surface areas. On one hand, the molecular dimensions of their pores (whose diameter varies between 3 and 20 Å, according to IUPAC definition of micropores) are close to kinetic diameter of many molecules, whose spatial conformation and/or electronic density distribution can be altered through the so-called confinement effect when they are adsorbed on such pores [3]. That physico-chemical alteration pre-activates the molecules in a so particular way that could determine the nature of the catalytically-formed product, that is, the selectivity of the catalytic reaction. On the other hand, the limited pore openings and the limited space inside of micropores introduced a new concept in catalytic selectivity, the so-called shape-selectivity [4] that groups different discrimination processes based on physical parameters (particularly on size) and not at all on any chemical property: only molecules with kinetic diameter smaller than pore entrances will react, only reaction intermediates with size and shape fitting in the void pore space will be formed, and only products smaller than pores could leave the pores and reach the reaction media.

Unfortunately, this set of a priori excellent advantages of microporous materials used as heterogeneous catalysts has found some serious limitations, which has reduced (or at least postponed) their massive industrial establishment. The most severe limitation is the restricted diffusion of reactants and/or products, provoked by the narrow fitting of these molecules in the pores and/or by the long path (pore length) to be travelled through them. It means that, paradoxically, the main limitation of zeolites and zeotypes for industrial applications comes from the property on which is based their own success: their microporosity [5]. Despite the main limitation and the main virtue of these materials have a common origin, intrinsically associated to the materials nature, different strategies have been proposed and/or developed with the aim of avoiding as much as possible the diffusion problems, renouncing as less as possible the confinement and the shape-selectivity given by microporosity. Some of these more successfully strategies are the following: zeolitic materials with higher pores [6,7]; non

short-range crystalline mesoporous materials with zeolitic [8] or zeotypic [9] composition; severe reduction of crystal size giving zeolitic materials composed by nano-crystals [10]; and mesoporous materials having walls composed by microporous nanocrystals [11], strategy somehow combining the three previous ones. Related to the latter, different methods to generate mesoporosity in microporous materials have been developed [12]. Such mesoporosity is intracrystalline if it is generated inside of the crystals, connecting micropores of a given crystal. Intercrystalline mesoporosity, the void mesosized space (of diameter between 20 and 500 Å, according to IUPAC classification of pores by size) delimited by nanocrystals (larger crystals would in principle delimit larger space, out of meso range), has been also described. The apparently necessary association of intracrystalline mesoporosity to nano-sized crystals implies the coexistence of two different factors that reduces the diffusion problems in the same material.

In a recent work [13], we showed that the structure directing agent (SDA) N-methyldicyclohexylamine (MCHA) is able not only to specifically direct the crystallization of AFI-structured $AlPO_4$-based materials but also to simultaneously generate intercrystalline mesoporosity delimited by nanocrystals without any extra mesopore-templating agent, almost irrespective of the nature of incorporated heteroatom ion. Nevertheless, the nature of such ions determined the morphology of the crystal aggregates and therefore their magnitude, distribution and size of the intercrystalline mesoporosity [13]. MCHA is not the only SDA able to direct intercrystalline mesoporosity in $AlPO_4$-5 materials without any extra mesopore directing agent [14]. However, its extraordinary specificity towards AFI materials, experimentally made clear in several publications [13,15-17] and theoretically justified [15,18], converts it to an appropriate candidate to carry out systematic studies with the guarantee of keeping constant the crystal structure. Complementing our previous work [13], this one focuses on a particular heteroatom ion, Co^{2+}, for studying the influence of different synthesis variables on the nature of the generated mesoporosity. The incorporation of Co^{2+} ions into the $AlPO_4$ frameworks is out of any doubt [19] and the catalytic activity of the CoAPOs has been studied in different reactions, particularly in the oxidation of hydrocarbons under environmentally benign conditions [20-22]. Some of the more influencing parameters resulted low pH values of the starting gel, Co content, crystallization time/temperature, gel dilution or heating source (conventional or microwave-assisted), whereas other parameters such as Co source nature or increasing pH above conventional value has no remarkable influence. The influence of each parameter is analyzed and discussed both individually and

collectively, in terms not only of the extension and type of mesoporosity but also of the crystal size, trying to establish the possible cause-effect relationship between them.

2. Experimental

2.1. Synthesis of CoAPO-5 materials

CoAPO-5 materials were prepared with two different structure directing agents (SDAs). Only one CoAPO-5 sample (CoAPO-5-TPA) of these discussed in this article were synthesized with tripropylamine (TPA), taking it as one of the SDAs conventionally directing AFI-structured $AlPO_4$-based materials. The experimental procedure for obtaining CoAPO-5 with this SDA was as follows. Cobalt (II) acetate tetrahydrate (purchased from Aldrich) was added over an aqueous phosphoric acid solution formed after the dilution of commercial H_3PO_4 85 % (Aldrich) with the whole water (Millipore grade) given by composition gel, which considers the amount of water inherently added with hydrated sources. Next, aluminum hydroxide hydrated ($Al(OH)_3 \cdot xH_2O$), purchased from Sigma, was slowly added over the pink solution, giving rise to a suspension of the same color. Finally, TPA (Aldrich) was added to complete the gel composition 0.96 Al : 0.04 Co : 1.0 P : 0.6 TPA : 60.0 H_2O. The purple mixture was keeping under vigorous stirring for one hour, and subsequently transferred into a Teflon-lined steel-stainless autoclave, where it was hydrothermally treated at 423 K for 18 hours under autogeneous pressure. The resultant samples, called in this article CoAPO-5-TPA, was filtered, washed with abundant amount of distilled water and dried at room temperature.

The rest of CoAPO-5 (Table 1) samples were prepared with MCHA as SDA. We took as starting point the CoAPO-5 sample whose mesoporosity nature has been already made clear [13]. The experimental procedure was described elsewhere [13] and exactly follows the above-described steps in the preparation of CoAPO-5-TPA. The only difference is the amount of some chemical sources (especially water) and the nature of SDA, to give the gel composition: 0.96 Al : 0.04 Co : 1.0 P : 0.8 MCHA : 25.0 H_2O. The hydrothermal treatment was at 448 K for 18 hours under autogeneous pressure. The so-called CoAPO-5-st (‘st’ for standard, as it will be taken as a reference in terms of crystallinity, crystal size, agglomerates morphology and especially mesoporosity) was recovered, filtered, washed with distilled water and dried at room temperature for at least 24 hours. Compared with these conditions, the following modifications were carried out in the preparation of the other CoAPO-5 samples synthesized with MCHA as SDA:

- Samples CoAPO-5-2h and CoAPO-5-4h: They were prepared from the same gel than CoAPO-5-st but hydrothermally treated for 2 and 4 hours, respectively, instead of 18 hours. The sample CoAPO-5-2h was separated from the whole solid, which is heterogeneous in color and appearance. Taking advantage of the higher density of the blue portion of the solid, all content of the autoclave was suspended into some distilled water under stirring for a few seconds, and subsequently left static for 30 seconds before being decanted. The deposited part is rich in the blue solid, whereas the decanted water carried the pinkish violet part of the solid, which was identified as amorphous by XRD. After repeating three times the suspension/decantation process, the blue solid was pure CoAPO-5, as confirmed by both XRD and SEM studies.
- Samples CoAPO-5-483K-2h and CoAPO-5-483K-18h: 483 K was the crystallization temperature at which these CoAPO-5 samples were prepared instead of 448 K at which CoAPO-5-st was crystallized.
- Samples CoAPO-5-2% and CoAPO-5-8%: instead of CoAPO-5-4%, which is the name that the sample CoAPO-5-st should take following the same nomenclature criteria: Co content of the gel was divided and multiplied by two, respectively, with respect to the Co content of the gel that generated the sample CoAPO-5-st. Al content of the gel was also modified as the general gel composition for any Co content was: 1-*x* Al : *x* Co : 1.0 P : 0.8 MCHA : 25.0 H_2O, where *x* was the Co/P ratio. These compositions were designed assuming that ions Co^{2+} will be exclusively incorporated into the sites occupied for Al^{3+} ions in a theoretical $AlPO_4$ framework. Added water was also modified in order to maintain the H_2O/P composition in a value of 25.0.
- Sample CoAPO-5-Cl: $CoCl_2 \cdot 6H_2O$: instead of Co(II) acetate tetrahydrate, was used as Co source. Water ratio in the gel composition was equally 25.0, so the amount of added water was slightly lower than in CoAPO-st.
- Samples CoAPO-5-0.5MCHA and CoAPO-5-1.6MCHA: A MCHA/P ratio of 0.5 and 1.6 were used, respectively, instead of that of 0.8 used for the gel that produced the crystallization of sample CoAPO-5-st.
- Sample CoAPO-5-5H_2O: This sample was crystallized from a gel equivalent to that generating the sample CoAPO-5-st, excepting the water content, which was that corresponding to a H_2O/P ratio of 5.0 instead of 25 for the starting

gel of the sample CoAPO-5-st. In both cases, the amount of added water was calculated discounting the water intrinsically added with the Co and P sources.

- Samples CoAPO-5-MW-1h, CoAPO-5-MW-1.5h and CoAPO-5-MW-4h: Heating assisted by microwave radiation instead of conventional heating was using for crystallization of these CoAPO-5, at the same temperature (448 K) and different crystallization times: 1, 1.5 and 4 hours, respectively. Unlike in conventional heating, during the microwave-assisted hydrothermal treatment the mixture was stirring at about 200 r.p.m. by magnetic agitation. The gel was treated inside of 100-mL Teflon-lined vessels and heating in a computer-controlled Milestone ETHOS ONE. Before crystallization time was started to be counted, a 20-minutes temperature ramp was used to reach crystallization temperature (448 K) from room temperature.

As-prepared samples were calcined at 813 K for 6 hours under an air flow of 30 $mLmin^{-1}$. Previously, the sample had been heating with a rate of 3 $Kmin^{-1}$ under a N_2 flow of 30 mL min^{-1} and maintained for 1 hour at 813 K under these atmosphere and flow.

2.2. Characterization techniques

Powder X-ray diffraction (XRD) patterns were acquired with a Philips X'PERT diffractometer using Cu Kα radiation. Difractograms were running with steps of 0.0167º, and each point was irradiated for 0.407 seconds. Crystallinity was calculated from the average of the area percentage of the reflections *210*, *002*, *211* and *220*, at ca. 19.7º, 21.0º, 22.4º and 25.9º, respectively, compared to those of the XRD pattern of the sample CoAPO-5-st, which was taken as 100 % crystalline. Crystallite sizes were estimated by applying Scherrer equation to the broadening of XRD reflections used to calculate crystallinity, taking advantage of their appreciable intensity. Alternatively, crystal size dimensions were estimated by Williamson-Hall plots. In particular, crystal widths *w* were calculated from origin ordinates of regression lines of Williamson-Hall plots for broadenings of the *h00* (*100*, *200* and *400*) and *00l* (*002* and *004*) XRD reflections [23]. More experimental details of this calculation were given elsewhere [13].

For Scanning Electron Microscopy (SEM) analysis, the samples were coated with a gold film before being observed in a field emission SEM (JEOL, SM-31010) equipment.

Nitrogen adsorption/desorption isotherms were measured at 77 K in a Micromeritics ASAP 2010 device. Before, as-prepared or calcined samples were degassed at 523 K or 623 K, respectively, under vacuum for at least 20 hours. Surface areas were estimated by BET method. Pore size distributions were obtained by application of BJH method to both adsorption and desorption branches of N_2 isotherms.

3. Results

3.1. Nature of SDA

Figure 1 compares the 2θ regions between 19º and 23º of the X-ray diffraction patterns of two samples CoAPO-5 of the same inorganic composition, prepared with TPA (sample CoAPO-5-TPA) and with MCHA (sample CoAPO-5-st) as SDAs. Both samples are exclusively composed by AFI material, what was confirmed by SEM studies. Supporting the absence of any amorphous impurity, the crystallinities of these two samples estimated by averaging the percentages of the peak areas of the four most intense reflections of the pattern are quite similar: 99.1 % for CoAPO-5-TPA and 100 % for CoAPO-5-st. However, the reflections of XRD pattern of the sample CoAPO-5-st are systematically much wider than these of the XRD pattern of the sample CoAPO-5-TPA, suggesting that the former is composed by crystals of smaller size. Such suggestion is evidenced by SEM images from Figure 2, which shows that CoAPO-5-TPA is formed by large isolated hexagonal crystals, whereas CoAPO-5-st is formed by micron-sized aggregates constituted by well-ordered crystals of micron-sized length and nano-sized width. Since crystal size and especially the aggregation capability of the crystals could be intuitively considered as key factors to generate intercrystalline mesoporosity, the differences between the N_2 adsorption/desorption isotherms at 77 K of both calcined CoAPO-5 samples (Figure 3), rather than becoming a surprise, are natural and simple consequences of what Figures 2 and 3 show. In micropore region, both isotherms are practically identical, adsorbing the same amount of nitrogen, again certifying the almost equal crystallinity of both CoAPO-5 samples. However, the isotherms are very different in the mesopore region: Whereas the shape of the isotherm of the sample CoAPO-5-TPA is the typical one of type I (IUPAC nomenclature [24]), with outstanding amount of nitrogen adsorbed in micropores but negligible amount of adsorbed nitrogen in mesopore and macropore regions, CoAPO-5-st also adsorbs/desorbs significant amounts of nitrogen at partial pressures at which mesopores are filled. Furthermore, the isotherm of CoAPO-5-st possesses a hysteresis loop (that is, adsorption and desorption branches follows different paths

along a pressure range, provoked by the different mechanism of pores filling and emptying with nitrogen gas), which is characteristic of mesopores. The nitrogen adsorbed amount by the mesopores of this sample, which is of similar magnitude to the amount adsorbed by its micropores, gives to the isotherm a type-II shape, according to IUPAC classification [24].

With the results of Figures 1-3 in mind, the systematic study of the influence of synthesis parameters on the nature of the intercrystalline mesoporosity and crystal size, has necessarily to be carried out with MCHA as SDA. Indeed, MCHA satisfies the three indispensable requirements associated to the aim of this work: i) a high specificity to AFI materials, which guarantees the obtaining of isostructural and pure materials when synthesis conditions are severely changed; ii) a tendency of producing AFI materials formed by crystals with at least one dimension of nano-size; and iii) an ability to generate intercrystalline mesoporosity through a particular crystal arrangement. As a consequence, the rest of the CoAPO-5 samples whose results are analysed and discussed along this article, were prepared with MCHA as SDA. At the beginning, we will show the effect of hydrothermal synthesis parameters (crystallization temperature and time), followed by parameters implying the alteration of chemical composition of the gel (Co content, Co source, MCHA content/pH of starting gel and H_2O content/gel dilution), and finishing with the change of conventional heating source by microwave-assisted one, which although would have been also considered as an additional hydrothermal synthesis parameter, we have preferred to analyse it separately because the use of microwave-assisted hydrothermal treatment influence not only on the crystal size of $AlPO_4$-based AFI-structured materials [25,26] but quite often transforms their mechanism of crystallization [25], and even changes the phase distribution [27] with respect to conventional heating.

3.2. Kinetics of crystallization

As above commented, it seems reasonable that intercrystalline mesoporosity should be favored when the samples are formed by nanocrystals rather than by crystals of micron-sized, since pores of mesosize (2-50 nm) are of the same size order than the nanodimension of the crystals responsible of generating such mesopores. At the same time, it is expected or, at least, probable that crystals after longer crystallization time are going to be of larger size. That is why we have centered our attention studying the influence of kinetics on the first stages of crystallization, when crystal growth is of scarce significance in comparison with the almost-completed nucleation by then.

The XRD patterns 2θ region (from 19 to 23 º) containing the three most intense reflections of the samples CoAPO-5-2h, CoAPO-5-4h and CoAPO-5-st, prepared from the same gel after being treated at 448 K for 2, 4 and 18 hours, respectively, are plotted in Figure 4. Surprisingly, some crystalline AFI material is already present after just two hours of hydrothermal treatment. That blue crystalline material, separated from the rest of solid, which is pinkish violet, by following the simple procedure described in experimental section, was about the 80 % p/p of the whole solid recuperated by filtration from the autoclave, the global solid yield being equal to the yields of the same gel treated for longer times. It means that at very short times of treatment crystallization is almost complete. The other two samples CoAPO-5-4h and CoAPO-5-st are composed by the all solid recovered by filtration, which was homogenously blue, evidencing the end of crystallization after 4 hours. In spite of so wide range of experimental conditions used in this paper, Co^{2+} ions were equally and rightly incorporated into $AlPO_4$-5 framework in all the samples discussed, according to the DR-UV-vis spectroscopic studies (not shown here). As expected, the XRD peaks width is generally reduced as crystallization time increases, evidencing that crystal size is effectively smaller at shorter crystallization times, and therefore either crystal growth or crystal blend follows the nucleation process if hydrothermal treatment is prolonged. In any case, this extremely quick kinetics of crystallization, together with the abundant nucleation (formation of nanocrystals), certifies that MCHA is not only a very specific SDA for AFI materials but it is also extraordinarily efficient.

The magnitude of the reduction of the XRD peaks width with the decrease of crystallization time, is not homogeneous along the whole difractogram but it depends on the *hkl* reflection. Thus, *002* reflection is practically not sensitive to the crystallization time, being relatively narrow in any case, whereas *210* and *211* peaks in the XRD pattern of CoAPO-5-2h are particularly broad. It implies that the longest (micron-sized) dimension of the crystals, which is already long when nucleation is the predominant crystallization process, is that along z-axis. Although that dimension cannot be accurately studied by methods that estimates crystal size from XRD peaks width, in principle it is not relevant for our aims as it is not a nano-dimension.

In spite of its short crystallization time, the sample CoAPO-5-2h is already formed by crystal agglomerates of phseudospherical shape, just like those described in CoAPO-5-st (Figure 2), and not by individual crystals that could agglomerate in a later step. Indeed, no isolated (not-agglomerated) crystals could be found in either the sample CoAPO-5-2h or the

residual all-amorphous solid from the same autoclave after several attempts with the FE-SEM equipments. It means that the crystal agglomeration/aggregation process (and presumably their associated mesoporosity generation) is simultaneously taken place with the nucleation. In other words, mesoporosity can be considered intrinsic to the existence itself of these MCHA-templated CoAPO-5 crystals.

SEM pictures (not shown) of these three samples did not show practically differences in the shape or size of the crystals agglomerates. However, according with XRD peak widths, SEM studies show a general trend of increasing crystal size with crystallization time, although there is no crystal size homogeneity within a given agglomerate and especially when different polycrystalline particles of a given sample are compared. In order to avoid any problem related to the lack of representiveness of the SEM technique, we will discuss the variation of crystal size and its effect on intracrystalline mesoporosity in this systematic series of samples based on estimations from XRD reflections width, taking advantage of the presence of crystals with a nanodimension (actually two, along the x- and y-axis). Due to the scarce accuracy of these estimations for micron-sized dimensions, data corresponding to crystal length is not even given. Table 2 compiles some relevant data arisen from XRD characterization of the samples CoAPO-5-2h, CoAPO-5-4h and CoAPO-5-st. We are aware that Scherrer method generally sub-estimates the crystal size at least for these AFI-structured materials [13], and it is not particularly appropriate for crystals of shape with very different dimension length (as for instance, the rod-like of these CoAPO-5 samples), since it gives just one average crystal size. However, we think that it is pertinent to qualitatively consider its estimations, due to its still widespread use and due to it has been applied in a series of systematic isostructural materials with similar crystal morphologies. Unlike Scherrer method, Williams-Hall one can give estimations of every crystal dimension if XRD reflections are strategically selected [13,23]. In any case, both Scherrer crystal size estimation and Williams-Hall crystal width estimation have parallel trends, both indicating that longer crystallization time is indeed associated with larger crystals width.

Figure 5 depicts the N_2 isotherms of the three CoAPO-5 samples prepared from the same gel but hydrothermally treated for different times. The isotherms of both calcined (top) and uncalcined (bottom) version of the samples are presented in the same Figure. The difference in the amount of N_2 adsorbed between the series of calcined samples and that of uncalcined ones is obviously due to the adsorption capacity of micropores, which are basically full of SDA molecules before calcination and basically void after calcination. The

amount of N_2 adsorbed by micropores of the sample CoAPO-5-2h is practically the same (or rather slightly higher) than that adsorbed by CoAPO-5-4h or by CoAPO-5-st. It confirms that the sample CoAPO-5-2h is as crystalline as their homologues. At first glance, calcination process does not introduce significant changes in mesoporosity, in good agreement with previous studies [13]. Preserving mesoporosity after calcination process is obviously an inescapable requirement of our work, which otherwise would be useless. Therefore, mesoporosity analysis should be equally valid from calcined or uncalcined samples. We will analyze the uncalcined series, simply because their trends, which are perfectly evident by comparing the isotherms of calcined ones, are even more systematic. Shortening crystallization times increases the global amount of mesoporosity and, at the same time, produces better defined mesoporosity, with mesopores of smaller sizes and with broader hysteresis loops. The interpretation of these experimental facts in terms of the geometry, concentration or distribution of mesopores as well as the number of conectivities between them is not direct. So many factors can influence on the N_2 adsorption/desorption over mesopores and sometimes the modification of some of these factors produces very similar effects on, for instance, the shape or magnitude of the hysteresis loop [24,28-30]. Thus, a widening of hysteresis loop could be related to a decrease of the connectivity number between pores [29,31], to a more extent mesopore network [29], to an effective compacting [30] or to smaller mesopore diameters [24,30]. Although all these explanations could be interpreted as distinct, the crystal growth described in this section could simultaneously explain some of them by itself, as it implies a reduction in pores connectivity, a more efficient crystal compacting and a reduction of mesopore size.

Some physical properties potentially affecting or related to the intracrystalline mesoporosity in this series of samples, estimated from XRD and N_2 adsorption measurements, are shown in Table 2. These data are somehow certain quantifications of what Figures 4 and 5 qualitatively show. Irrespective of the method used for estimating the crystal size from XRD peaks widths, it is evident that crystal size increases along crystallization time. That crystal size increase is accompanied by a systematic decrease of external surface area, a systematic increase of BJH pore size distribution (PSD) estimated from both adsorption and desorption branches, and a systematic decrease of mesopore volume. All these facts suggest that some extent of crystal growth follows the nucleation process, in spite of the massive nucleation taken place in a short crystallization period. The increase of crystal size without the increase of agglomerate size implies that, given the type of crystal arrangement in the agglomerates

shown in Figure 2, nano-dimension and not micron-dimension of the crystals grows with crystallization time. This crystal broadening without lengthening explains the reduction of both surface area and void volume of the mesopores. Regarding the parallel and apparently contradictory increase of PSD maximum with crystallization time, it could be explained taking into account that PSD distribution is an average evaluation. Crystal growth could eliminate the mesopores or to make them inaccessible to N_2, whereas the largest mesopores would be scarcely reduced, proportionally speaking, still being large and now predominant in volume and probably also in abundance. The evolution of the isotherms shape (Figure 5) along crystallization process strongly supports this hypothesis.

3.3. Crystallization temperature

Like crystallization time, hydrothermal treatment temperature is one of the parameters being always considered in any crystallization process. Since the mechanism of zeolites/zeotypes formation is varied (solid-to-solid, liquid-to-solid, supramolecular assembly, etc.) and complex (metastable phases, often co-crystallization of more than one phase, role of structure-directing agents and/or alkali cations, different reactions involved such as hydrolysis or condensations, possible role of heteroatom ions, etc.), the approach of the general theory of crystallization is hardly predictable and rarely applied to these materials. Nevertheless, it seems reasonable that in our system higher temperatures should favor the massive and an almost simultaneous nucleation in different points of the gel, generating smaller crystals which can be easily arranged in agglomerates having intercrystalline mesoporosity.

With this idea in mind and especially taking into account our previous experience with the system CoAPO-5/MCHA, we decided to prepare CoAPO-5 samples only at one temperature (483 K) higher than the standard one (448 K) as possible alternative based on modification of crystallization temperature to improve the mesoporosity in this material. Since shorter crystallization times seem to favor the generation of well-defined mesoporosity, according to the 3.2 section, we included 2 hours, besides 18 hours, as an extra crystallization time at 483 K. The two resultant samples were called CoAPO-5-483K-2h and CoAPO-5-483K-18h. XRD patterns (not shown) indicated that the sample CoAPO-5-483K-2h, which unlike CoAPO-5-2h was formed by the whole solid from the autoclave, is pure and highly-crystalline CoAPO-5, indicating that these hydrothermal conditions (483 K, 2 hours) are enough to complete the crystallization. On the contrary, although the sample CoAPO-5-483K-18h was mainly formed by the AFI-structured phase, a crystalline impurity, presumably of a

dense (non-porous) material as its XRD peak of lowest angle was found at ca. 21.8º. As aimed, the XRD reflections are slightly wider. However, the reduction in crystal size does not compensate the increasing uncertainness for optimizing crystallization time or the probable co-crystallization of dense impurities, both problems associated to higher crystallization temperatures.

Figure 6 displays the isotherms of four uncalcined CoAPO-5 samples: CoAPO-5-483K-2h and CoAPO-5-483K-18h and their homologues prepared at 448 K, that is, the samples CoAPO-5-2h and CoAPO-5-st, whose isotherms were already presented in Figure 5. The general evolution of the isotherms shape with the severity of the hydrothermal treatment (considering severe treatment either those after very long crystallization times or those at very high temperatures) strongly resembles that shown in Figure 5, where only crystallization time was varied. In other words, increasing crystallization temperature has a very similar effect to that provoked by prolonged crystallization times. Therefore, the effect of both crystallization time and temperature can be grouped in a common effect which could be called as heating treatment.

3.4. Cobalt content

The samples called CoAPO-5-2%, CoAPO-5-st and CoAPO-5-8% form a systematic series as they were prepared by just changing the Co content *x* (and accordingly the Al content 1-*x*) of the respective gels with general composition 1-*x* Al : *x* Co : 1.0 P : 0.8 MCHA : 25.0 H_2O, where *x* was the Co/P molar ratio in the gel, having values of 0.02, 0.04 and 0.08, respectively. At first glance, their XRD patterns (not shown), including the peak widths, are quite similar, suggesting that the crystal size does not strongly depend on the Co content. Figure 7 shows a SEM picture of every sample of the series, with different magnification since they were selected in order to show the size and shape of a representative particle of each sample. The particles constituting the CoAPO-5 samples systematically change both their particle morphology and size with Co content. The morphology changes were already described [13] by just comparing the cylindrical shape of the $AlPO_4$-5 particles with the pseudospherical one of the CoAPO-5, here called CoAPO-5-st. The morphology of the sample CoAPO-5-2% would be the ‘missing link’ between both mentioned samples, and indeed its crystals agglomerates posses a morphology of mushroom-like double-lobe shape, which could be considered as intermediate between the cylindrical shape of $AlPO_4$-5 and the pseudospherical one of CoAPO-5-st. Consistently with this morphology evolution, the

morphology of the sample CoAPO-5-8% is completely spherical, even more than that of the CoAPO-5-st crystals in whose pseudospherical particles can be still detected the presence of two lobes.

Figure 8 shows the N_2 adsorption/desorption isotherms at 77 K of the three uncalcined CoAPO-5 samples with different Co content, after being evacuated at 573 K for at least 20 hours. The isotherm of an $AlPO_4$-5 sample, prepared as described elsewhere [13] under similar conditions to these used for the three CoAPOs, is also shown for comparison proposes. The most visible difference between these four isotherms is the amount of N_2 adsorbed by the micropores, which is almost negligible for the standard sample CoAPO-5-4% and for the sample CoAPO-5-8%, whereas it is significant in the case of the sample CoAPO-5-2% and outstanding (near the amount expected for a calcined AFI material) for $AlPO_4$-5. The reason of this evolution of N_2 adsorbed with micropores must be related to the different role of MCHA located inside of the pores. Thus, in samples relatively rich in Co, MCHA compensates the charge associated to the incorporation of Co^{2+} ions in Al^{3+} sites, and therefore this SDA has to be protonated and quite strongly retained. In contrast, MCHA and /or water are simply filling the pores of $AlPO_4$-5 as no charge has to be compensated, so they are easily removed under evacuation conditions, leaving void a substantial part of micropores. Since TGA analyses (not shown) certifies that the amount of MCHA in $AlPO_4$-5 is, although slightly lower, almost equal to that contained in CoAPO-5 samples, an important amount of MCHA is removed from micropores.

Apart from liberated void in micropores, there is another systematic variation as a function of the Co content of the sample. Unlike the previous trend, this one is directly related to the mesoporosity nature, the issue of this article. It consists on the systematic evolution of the shape of the hysteresis loop, which is very poor-defined and even does not close in the isotherms of the $AlPO_4$-5 and CoAPO-5-2% samples, but is perfectly delimited in the isotherms of the two Co-richer samples. The unclosed hysteresis loop is not so uncommon in bibliography [32,33], although it has been rarely explained. According to IUPAC [24], this phenomenon may be associated with the swelling of a non-rigid porous structure or with the irreversible uptake of molecules in pores (or through pore entrances) of about the same width as that of the adsorbate molecule or in some instances with an irreversible chemical interaction of the adsorbate with the adsorbent. Considering the nature of our samples and particularly of their intracrystalline mesoporosity, the presence of non-rigid porous structure seems to be the most probably reason of the unclosed isotherms. If so, it means that high Co

content of the sample somehow gives an extra mechanical consistency to the crystal ordering, supported by SEM images (Figure 7), which evidences that an increase of Co content is associated to agglomerates of larger size and more spherical shape, both characteristics intuitively contributing to enhance the mechanical stability of the aggregates and therefore that of their intercrystalline mesoporosity.

3.5. Co source

Unlike some other heteroatom ions, Co^{2+} appears to have a relevant role in the crystallization mechanism of the CoAPO-5 material [13]. Accordingly, the previous section 3.4 of this article made clear that the amount of Co in the starting aluminophosphate-based gel determines the size and even the mechanical stability of the crystal agglomerates and, consequently, the nature of the intracrystalline mesoporosity. In this sense, some influence of the Co source on the generated mesorporsity should not be ruled out.

Although nowadays Co(II) acetate is probably the most used Co source in the preparation of CoAPOs, the first CoAPOs were prepared with Co(II) sources whose counter-anions were very weak bases such as Cl^- or NO_3^-. Potentially, that chemical distinctiveness could have some influence in the intracrystalline mesoporosity, and therefore we prepared a CoAPO-5 using $CoCl_2$ as Co source. However, the so-called CoAPO-5-Cl resulted to be a sample with almost the same properties than those of CoAPO-5-st (prepared with Co(II) acetate), at least in terms of phase purity, crystal size and shape, crystal agglomerates size and shape and magnitude and nature of their micro- and mesopores. Therefore, showing characterization results of the sample CoAPO-5-Cl is not worth, but we consider important to mention that the influence of Co(II) sources on the mesoporosity in this system is negligible, at least for the two studied Co sources.

3.6. pH of the starting gel: SDA content

The role of structure-directing agents (SDAs) in the formation of microporous materials continues being unknown in some aspects [34-37]. Although during decades they were called templates in the context of zeolites [38], following the attributed role to them at that time, their general low specificity (of which MCHA is an exception) in $AlPO_4$-based materials makes clear that so many times the sizes and shapes of SDAs becomes secondary in comparison with the effect of some other parameters. Undoubtedly, one of these most structural influencing parameters is the pH value of the starting gel. Fortunately, MCHA is

able to selectively direct AFI-structured $AlPO_4$-based materials in a relatively wide range of pH values, allowing us to study the pH effect on other properties of the obtaining materials, different to their structure-directing role, such as intercrystalline mesorporosity. In general, the variation of pH values of the starting gels along a series of experiments is designed by altering the ratio of some (normally, just one) species already present in the standard gel composition. In this way, the unpredictable role of extra species such as strong bases, strong acids or pH tampons has been avoided in this work. In this context, we have decided to modify the pH of the starting gel with different amounts of MCHA instead of, for instance, those of phosphoric acid, which would alter the ratio between inorganic species that forms the zeotype framework.

The samples CoAPO-5-1.6MCHA, CoAPO-5-st and CoAPO-5-0.5MCHA were prepared under the same conditions and starting from gels with similar compositions, excepting in the ratio MCHA/P, which was 1.6, 0.8 and 0.5, respectively. As a consequence of this difference in gel composition, their pH values before hydrothermal treatment were 8.8, 6.9 and 5.1, respectively. The samples CoAPO-5-1.6MCHA and CoAPO-5-st resulted very similar in their characterization by a large number of techniques, including XRD, N_2 isotherms and SEM. Therefore, in spite of important differences in pH of their starting gels, these two samples are composed by crystals of similar size agglomerated in particles of similar morphology, size and nature of intracrystalline mesoporosity. That is why no results will be hereafter shown, commented or discussed about the sample CoAPO-5-1.6MCHA. CoAPO-5-st is taken as the representative CoAPO-5 sample prepared at high pH, and it will be compared with CoAPO-5-0.5MCHA, prepared at low pH.

Figure 9 shows the 2θ region between 19º and 23º of the normalized XRD patterns of the samples CoAPO-5-st and CoAPO-5-0.5MCHA. It is clear that the peaks of the XRD pattern of CoAPO-5-st are significantly broader, suggesting that lower pH leads to a CoAPO-5 material with larger crystals. Effectively, SEM images (Figure 10) of the sample CoAPO-5-0.5MCHA show that it is formed by crystals with all their dimensions clearly above the nano range. However, they are perfectly compacted in the agglomerates, so the presence of mesoporosity should not be a priory ruled out.

The isotherms of the uncalcined samples CoAPO-5-st and CoAPO-5-0.5MCHA are compared in Figure 11. According to the isotherms shapes, it is obvious that both samples posses certain mesorporosity but of different nature and magnitude. Attending to the N_2 adsorbed on mesopores, the standard CoAPO-5 is richer in mesoporosity, as expected

considering that the big crystal size of the sample CoAPO-5-0.5MCHA in principle cause some doubts about the possibility of this sample has any mesoporosity. In addition, the excellent crystal compacting showed in Figure 10 implies that, admitting the existence of some mesoporosity, the ratio mesorporosity/mass of CoAPO-5 should be really low. On the other hand, the isotherm of CoAPO-5-0.5MCHA suggests that the average mesopore is of smaller diameter than that of the CoAPO-5-st, suggestion that was confirmed by their PSD maxima (25.6 nm for the adsorption branch and 10.0 nm for the desorption branch against 30.4 and 18.0 nm of the corresponding homologues values for the isotherm of the sample CoAPO-5-st (Table 2)) [30]. This fact makes clear once again the effective compacting reaching by the so large crystals of the sample CoAPO-5-0.5MCHA. Finally, another difference in shape between the isotherms compared in Figure 11 is the presence of a plateau at high partial pressures in the sample CoAPO-5-0.5MCHA, which is absent in the isotherm of the CoAPO-5-st, so that the corresponding hysteresis loops should be classified of different type: type H2 for the isotherm of CoAPO-5-0.5MCHA and type H3 for the isotherm of CoAPO-5-st. It is admitted that hysteresis loops of type H3 is due to the presence of plate-like particles giving rise to slit-shaped pores [24]. In contrast, the hysteresis loops of type H2 is generally associated to more or less longitudinal channels, with limited connectivity, in good agreement with the pores that can be formed in the agglomerates shown in Figure 9.

3.7. Gel dilution

As pointed out in section 3.4., the conventional theory of crystallization should not be applied to the crystallization of microporous materials, due to certain peculiarities of these systems. Nevertheless, gel dilution/concentration has been often used, for instance, in the control of crystal size in microporous materials. Accordingly, water content of the gels generating CoAPO-5 with MCHA as SDA could potentially alter the intercrystalline mesoporosity in these systems.

In contrast to the standard sample CoAPO-5-st, prepared with a H_2O/P ratio of 25, the sample CoAPO-5-5H_2O crystallized from a gel with H_2O/P ratio of 5, very close to the minimum value, taking into account that some chemical sources such as H_3PO_4 and Co(II) acetate inherently provides some water to the gel, already included in the above-given H_2O/P ratios. The sample was mainly constituted by AFI phase, although a crystalline impurity of a presumable non-microporous (first reflection in the XRD pattern was for a 2θ above 20º) material was also present, and whose morphology was identified and easily distinguished by

SEM studies. SEM pictures of Figure 12 showed regions of the sample in which there was no evidence of that crystalline impurity. Like in the case of CoAPO-5-st, the sample CoAPO-5-5H_2O is composed by hexagonal crystals having a dimension of nano-size (considering nano-dimension below 100 nm). These crystals appear to have certain tendency to be agglomerated. Even, seen with low magnification, some of those agglomerates are pseudo-spherical, slightly resembling these of some other CoAPO-5 samples previously shown (Figures 2-right, 7 and 10). However, either these pseudo-spherical or shapeless particles, although both formed by a large number of AFI crystals, are far from reaching the exceptional orderly arrangement of the crystals in any other CoAPO-5 prepared with MCHA and with a H_2O/P ratio of 25, which confers them a very regular shape and a relatively ordered intercrystalline mesorporosity.

Figure 13 compares the isotherms of as-prepared CoAPO-5-5H_2O and CoAPO-5-st. In this case, we have decided to compare the as-prepared samples for two reasons: i) the presence of impurities in CoAPO-5H_2O, making strictly incomparable their microporosity, and overall, ii) the unpredictable effect of calcination process on the mechanical stability of CoAPO-5-5H_2O particles, which are apparently weak pile of crystals. Like the isotherm of the CoAPO-5-st sample, that of CoAPO-5-5H_2O possesses certain void mesoscopic space but it does not show any hysteresis loop, suggesting the absence of mesopores. In other words, in good agreement with the SEM images from Figure 12, the void space left by the agglomeration of AFI-structured crystals in the sample CoAPO-5-5H_2O is of mesoscopic dimension, as expected considering the crystal size and a certain trend of the AFI crystals to form agglomerates, but this void space is not ordered nor periodical at all and is not given by meso-channels.

3.8. Heating source

In so many examples in literature, the microwave-assisted hydrothermal treatment has been used to decrease and/or homogenize the crystal size of $AlPO_4$-based microporous materials [26,39,40]. Taking into account the origin of the intercrystalline mesoporosity in our CoAPO-5 system, it is evident that smaller and more homogeneous crystal size will reduce the diffusional problems of these materials, so they would improve their catalytic features.

The samples CoAPO-5-MW were prepared under hydrothermal treatment assisted by microwave radiation, starting from a gel identical to that generated CoAPO-5-st by conventional (and convectional) hydrothermal heating. In both cases, the temperature was 448 K. However, it is well-known that microwave-assisted treatment generally accelerates the

crystallization process, so maintaining the same crystallization time with both heating sources is not precisely a guarantee of systematicity in this case. Since the kinetics described in section 3.2. cannot even use as a reference of crystallization time, we studied the own kinetics for microwave-assisted heating.

Figure 14 shows the *210* reflections of XRD patterns of the samples CoAPO-5-MW-1h, CoAPO-5-MW-1.5h and CoAPO-5-MW-4h, prepared under heating given by microwave radiation, compared with the same reflection of the XRD pattern of the sample CoAPO-5-st, as standard reference along this article, and with that of the sample CoAPO-5-2h, as sample prepared with conventional heating having the smallest crystals (broadest XRD reflections). The choice of *210* reflection is justified because it is one of the most intense reflections, what minimizes the error in the width measurement, and because it is particularly and exclusively sensitive to the nano-dimensions, along *x* and *y* crystallographic axis. The slight shift in 2θ should be probably due to some experimental inaccuracy in 2θ alignment or in sample preparation. The whole crystallization of the CoAPO-5-MW samples occurs between 0.5 hours (at that time, only pink amorphous samples could be obtained from the autoclave) and 1 hour, after which only homogenous, pure and crystalline blue CoAPO-5 sample is afforded. Since the crystallization under conventional heating needed more than 2 hours to be completed, microwave-assisted heating accelerates the kinetics of crystallization. The XRD reflections width of the CoAPO-5-MW-1h pattern (*210* reflection FWHM of 0.251 º) is very much broader than that of the XRD pattern of CoAPO-5-st (0.190 º) and quite similar or even slightly broader than that of CoAPO-5-2h (0.236º). An increase of crystallization time, relatively important considering that it is under microwave-assisted heating, produces very little changes in the *210* reflection width, which is of 0.234 º for CoAPO-5-MW-1.5h and 0.235 º for CoAPO-5-MW-4h. So, unlike conventional heating, there is no a significant crystal growth for prolonged crystallization times, probably because their most effective nucleation consumes practically all inorganic nutrients from the gel.

In Figure 15, some SEM images of the sample CoAPO-5-MW-1h are shown. The sample was homogeneous and formed by pseudospherical highly-ordered crystals agglomerates, sometimes fuses together as, for instance, the portion of the sample in the image with lower magnification from Figure 15. We were not able to localize any portion of the sample not responding to this pattern, confirming that the crystallization was finished after just one hour of hydrothermal treatment. From the image registered with higher magnification, and in good agreement with the broad XRD reflections (Figure 14), it is

evident that the crystals are smaller than those forming, for instance, the sample CoAPO-5-st (Figure 2), fulfilling the proposed objective with this heating source

As in previous sections, intercrystalline mesoporosity is deeply analyzed by N_2 adsorption/desorption isotherms at 77 K. Figure 16 shows the isotherms of four as-prepared CoAPO-5 materials, these corresponding to the shortest and longest crystallization time for each of the two heating sources. On one hand, shortest crystallization times of different heating sources and, on the other hand, longest ones have similar mesopore volume, although of different nature. In general, samples synthesized in microwave oven have better defined and smaller mesopores. In addition, the crystallization time seems to provoke changes of similar trends but much marked under conventional heating. In both cases, these changes should be related to the crystal growth process, in spite of XRD reflections width analysis in the case of microwave-assisted heating suggests that, if any, it is given in a low extent. Indeed, the PSD maximum from adsorption branches is not changed between the CoAPO-5-MW included in Figure 16, and the decrease of PSD maximum of desorption branches with crystallization time is very minor, from 16 to 19 nm, in contrast with the series of CoAPO-5 samples prepared under conventional heating (Table 2). In short, microwave-assisted heating offers us a larger margin to stop the crystallization reaction conserving almost all mesorporosity, which in addition will be of smaller size for a similar pore volume, that is, there should give higher (mesopores number/micropores number) ratio for a similar (mesopore volume/micropore volume) ratio, what means an important advantage for diffusion.

4. Discussion

From analyses of Figures 1-3, it is clear that the generation of intercrystalline mesoporosity without any mesostructure-directing agent in $AlPO_4$-based materials is far from being universal. Therefore, the structure-directing agent nature (in principle, selected according to their capacity to direct a specific microporous framework) plays an essential role. Based on some intuitive requirements for generating intercrystalline mesoporosity such as presence of nanocrystals and their tendency to be orderly agglomerated or aggregated, it seems perceptible that a good SDA for this propose must be: i) very specific towards the structure of the material of interest in order to favour the nucleation process (*versus* crystal

growth); ii) able to quickly and homogenously crystallize the material in order to disfavour the crystal growth (*versus* nucleation); and iii) not easily miscible with water (or with the solvent, in general), even reaching a pseudo or real biphasic media, which leads to local domains (emulsions) with high concentration of SDA, in order to favour the crystal aggregation (closer nucleation points) and, at the same time, disfavour the crystal growth (slower supply of nutrients from one phase to another). In this context, comparing the two SDAs of this study, MCHA is more specific to AFI-structured materials [13,15], gives them with a quicker kinetics, and it is less miscible with water (sometimes, two liquid phases are appreciable both before and after of the hydrothermal treatment, especially at high concentration of MCHA), as it can be deduced from its bulkier hydrocarbon chains, which not only would give to MCHA molecule a higher hydrophobic character but also would contribute to hide the most polar part (the N atom) by steric impediments.

The different CoAPO-5 samples obtaining by following the kinetics of crystallization showed a good correlation between the crystal size (or their external non-microporous surface area) and the amount of adsorbed N_2 in mesoporous region (Table 2). That tendency corroborates the convenience of favouring nucleation against crystal growth (in this case, shortening the crystallization time) to efficiently produce mesoporosity. In fact, such mesoporosity is extraordinarily sensitive to the crystallization time. Thus, carrying out the synthesis at 448 K, 2 hours of crystallization time is not enough to avoid the presence of non-reacted amorphous solid part, and prolonged the crystallization up to 4 hours already means a notable loss of mesoporosity. On the other hand, increasing crystallization temperature up to 483 K scarcely reduced the crystal size, confirming that favouring nucleation is at beneficial. However, it accelerated at the same time the degradation of the mesoporosity making more difficult to optimize the crystallization time, which together with the presence of dense crystalline impurities makes inappropriate their use against lower temperatures as 448 K.

The differences in agglomerates morphology and the similarities in crystal size and morphology between the samples CoAPO-5-st and CoAPO-5-5H_2O confirms that the aqueous phase/organic phase ratio plays an important role in the agglomeration/aggregation of the crystals and therefore in their intercrystalline mesopority. A possible explanation can be given admitting that nucleation takes place in the organic-rich phase but the agglomeration in the hydrophobic-hydrophilic interfaces, that is, it is somehow due to the presence of (pseudo)emulsions. In the viscous gel generating the sample CoAPO-5-5H_2O, great and non-defined organic domains rather than small, spherical and relatively homogeneous emulsions

could be formed. If so, the nucleation would be scarcely affected but the crystals formed would not have any chance to reach an ordered arrangement. This fact would invite us to include a fourth requirement for a good SDA for searched proposes: it not enough with forming agglomerates but they should be highly ordered and preferably compacted; in other words, the particles grouping crystals should be aggregates (with strong links between crystals which ideally should fuse amongst them) rather than simple agglomerates (just linked by SDA molecules or by weak interaction forces between crystal surfaces).

In this context, the crystals formed at low pH were not expected to form mesoporosity as their size is too large. However, relatively acidic conditions seems to favour the formation of compact crystal aggregates or at least highly ordered agglomerates which would allow that later crystal growth process gives them extraordinary robustness. This possible mechanism would be the responsible of forming intracrystalline mesoporosity of size of at least one magnitude order higher than that of the crystals delimiting it. Therefore, although the three above-cited requirements for a good SDA to efficiently generate intercrystalline mesoporosity in microporous materials could be a good starting guide, they could not be taken as strict. Thus, the assumption that reducing crystal size automatically implies an improvement in mesoporosity is not universally applied, at least not in terms of narrower mesopores.

The only parameter whose influence over the mesoporosity has been studied in this article that affects the properties of the final CoAPO-5 material (composition, number of actives centres, etc.) is the Co content. Therefore, it should be taken carefully as strategy for limiting diffusional problems. Co(II) ions participation in crystallization of CoAPO-5 in this system has been strongly suggested [13] and supported in this article by their alteration of the aggregates morphology (Figure 7) and, accordingly, on the intracrystalline mesoporosity. Low Co content produces materials tending but not reaching spherical agglomerates, with void pores of meso size very interconnected amongst them, so they are not channels properly speaking. Higher Co content progressively increases the agglomerates size, which are becoming of spherical shape, and more importantly, the hysteresis loop shapes of the isotherms strongly suggest that the pores tend to be more defined and probably are losing some interconnectivities, being closer to reach the meso-sized channel conditions.

As expected, the use of microwave-assisted heating favors the obtaining of smaller and more homogeneous CoAPO-5 crystals. Unlike the unpredictable changes in mesoporosity introduced by decreasing the pH of starting gel, in this case the decrease of crystal size predictably favors the smaller size of the intracrystalline mesopores as well as provides a

better defined mesoporosity. It probably converts the strategy of using hydrothermal treatment induced by microwave radiation in the most promising approach in the generation and control of intracrystalline mesoporosity. In this sense, one could propose to repeat all this study but now taken as the standard sample one prepared under microwave radiation, assuming that crystallization process nature changes depending on the heating source, as suggested by the evolution of mesoporosity with crystallization time, the only parameter studied. However, in our opinion, the general tendencies in this article can be quite probably extrapolated to a microwave radiation media. In any case, there are so many parameters influencing the intercrystalline mesoporosity, which can be potentially interconnected each others. In this context, we are aware that the tendencies arisen from the different sections 3.n. have been established individually, from a simple comparison with the so-called standard sample CoAPO-5. Therefore, an appropriate statistical design of experiments should help to select even better conditions for intracrystalline mesoporosity or, more ambitiously, the best conditions for avoiding diffusional problems in these CoAPO-5 materials.

5. Conclusions

This article examines the influence of certain synthesis parameters on the extension and nature of intracrystalline mesoporosity in CoAPO-5 materials prepared with N-methyldicyclohexylamine (MCHA) as structure-directing agent. Some of these parameters such as crystallization time, crystallization temperature or heteroatom content have a moderate effect; some others such as certain values of pH or gel dilution/concentration have a more significant effect; and Co source has no effect. Moreover, not every parameter modifies the same properties of intracrystalline mesoporosity. On the contrary, depending on the changed parameter, mesoporosity could modify one or several aspects as diverse as mesopore size diameter and distribution, mesopore connectivities, mesopore flexibility or mesopore volume magnitude. Thus, the extension and periodicity of the intracrystalline mesoporosity improves at short crystallization times (2 hours, in this article), at the highest tested crystallization temperature (483 K), at the highest tested Co content (8 molar % Co in Al sites), at the lowest tested pH of the starting gels (at pH *ca.* of 5), and at the highest tested dilution (H_2O/P ratio of 25). However, the main improvement of the mesoporosity properties was found by changing the conventional heating by microwave-assisted one. Maintaining the morphology of the AFI crystals and their agglomerates with respect to the conventional hydrothermal treatment, heating by microwave irradiation decrease and homogenize crystal

width, and generates more ordered mesoporosity of smaller pores. In summary, although this work establishes the bases for the experimental control of the intracrystalline mesoporosity in this particular system, at the same time open more exciting possibilities by extending the studied parameter at more extreme values, by introducing new ones and by combining some different proposed strategies.

Above all these results, it is fair to mark the ability of MCHA to produce CoAPO-5 materials with a high specificity and with intracrystalline mesoporosity, of nature and magnitude variable, under a truly wide range of conditions. The possibility of broadly modifying the extension and the type of mesoporosity in this system by just changing more or less rationally the synthesis parameters opens new routes and/or strategies for designing microporous materials with minimized diffusional problems.

Acknowledgements

Authors acknowledge Spanish Science and Innovation Ministry for financial support (MAT-2009-13569).

References

[1] A. Corma, J. Catal. 216 (2003) 298–312.

[2] A.F. Masters, T. Maschmeyer, Microporous Mesoporous Mater. 142 (2011) 423-438.

[3] J. Sivaguru, A. Natarajan, L.S. Kaanumalle, J. Shailaja, S. Uppili, A. Joy, V. Ramamurthy, Acc. Chem. Res. 36 (2003) 509-521.

[4] S.M. Csicsery, Zeolites 4 (1984) 202-213.

[5] J.C. Groen, L.A.A. Pfeffer, J. Perez-Ramirez, Micropor. Mesopor. Mater. 60 (2003) 1.

[6] M.E. Davis, C. Saldarriaga, C. Montes, J. Garces, C. Crowder, Nature 331 (1988) 698-699.

[7] J.L. Sun, C. Bonneau, A. Cantin, A. Corma, M.J. Diaz-Cabanas, M. Moliner, D.L. Zhang, M.R. Li, X.D. Zou, Nature 458 (2009) 1154-1157.

[8] C.T. Kresge, M.E. Leonowicz, W.J. Roth, J.C. Vartuli, J.S. Beck, Nature 359 (1992) 710-712.

[9] B.T. Holland, P.K: Isbester, C.F. Blanford, E.J. Munson, A. Stein, J. Am. Chem. Soc. 119 (1997) 6796-6803.

[10] I. Schmidt, C. Madsen, C.J.H. Jacobsen, Inorg. Chem. 39 (2000) 2279-2283.
[11] A. Karlsson, M. Stocker, R. Schmidt, Microporous Mesoporous Mater. 27 (1999) 181-192.
[12] K. Egeblad, C.H. Christensen, M. Kustova, C.H. Christensen, Chem. Mater. 20 (2008) 946-960.
[13] A. Manjon-Sanz, M. Sanchez-Sanchez, P. Muñoz-Gomez, R. Garcia, E. Sastre, Microporous Mesoporous Mater. 131 (2010) 331-341.
[14] J. Wang, J. Song, C. Yin, Y. Ji, Y. Zou, F.S. Xiao, Microporous Mesoporous Mater. 117 (2009) 561-569.
[15] M. Sanchez-Sanchez, G. Sankar, A. Simperler, R.G. Bell, C.R.A. Catlow, Catal. Lett. 88 (2003) 163-167.
[16] R. Roldan, M. Sanchez-Sanchez, G. Sankar, F.J. Romero-Salguero, C. Jimenez-Sanchidrian, Micropor. Mesopor. Mater. 99 (2007) 288-298.
[17] M. Sanchez-Sanchez, R. van Grieken, D.P. Serrano, J.A. Melero, J. Mater. Chem. 19 (2009) 6833-6841.
[18] M. Sanchez-Sanchez, G. Sankar, Stud. Surf. Sci. Catal. 154 (2004) 1021-1027.
[19] B.M. Weckhuysen, R.R. Rao, J.A. Martens, R.A. Schoonheydt, Eur. J. Inorg. Chem. 4, (1999) 565-577.
[20] J.M. Thomas, R. Raja, G. Sankar, R.G. Bell, Nature 398 (1999) 227-230.
[21] J.M. Thomas, R. Raja, G. Sankar, R.G. Bell, Acc. Chem. Res. 34 (2001) 191-200.
[22] R. Raja, S.O. Lee, M. Sanchez-Sanchez, G. Sankar, K.D.M. Harris, B.F.G. Johnson, J.M. Thomas, Top. Catal. 20 (2002) 85-88.
[23] A.W. Burton, K. Ong, T. Rea, I.Y. Chan, Micropor. Mesopor. Mater. 117 (2009) 75-90.
[24] K.S.W. Sing, D.H. Everett, R.A.W. Haul, L. Moscou, R.A. Pierotti, J. Rouquerol, R. Siemieniewska, Pure Appl. Chem. 57 (1985) 603-619.
[25] I. Girnus, K. Jancke, R. Vetter, J. Richtermendau, J. Caro, Zeolites 15 (1995) 33-39.
[26] H.B. Du, M. Fang, W.G. Xu, X.P. Meng, W.Q. Pang, J. Mater. Chem. 7 (1997) 551-555.
[27] S.H. Jhung, J.H. Lee, J.W. Yoon, J.S. Hwang, S.E. Park, J.S. Chang, Microporous Mesoporous Mater. 80 (2005) 147-152.
[28] S.J. Gregg, K. S.Sing, 'Adsorption, Surface Area and Porosity', Second Edition, Academic Press (1982).
[29] D.K. Epremov, V.B. Penlonov, Stud. Surf. Sci. Catal. 62 (1991) 115-122.
[30] PhD Thesis, R. H. López, Universidad Nacional de San Luis, Argentina (2004).

[31] S. Cordero, A. Dominguez, I. Kornhauser, R.H. Lopez, F. Rojas, A.M. Vidales, G. Zgrablich, Colloids Surf. A: Physicochem. Eng. Aspects 241 (2004) 47–52.
[32] M.C. Burleigh, M.A. Markowitz, M. S. Spector, B. P. Gaber, J. Phys. Chem. B 105 (2001) 9935-9942.
[33] C. Li, J. Yang, X. Shi, J. Liu, Q. Yang, Microporous Mesoporous Mater. 98 (2007) 220–226.
[34] C.S Cundy, P.A. Cox, Microporous Mesoporous Mater. 82 (2005) 1-78.
[35] J.H. Yu, R.R. Xu, Chem. Soc. Rev. 35 (2006) 593-604.
[36] M.G. O'Brien, M. Sanchez-Sanchez, A.M. Beale, D.W. Lewis, G. Sankar, C.R.A. Catlow, J. Phys. Chem. C. 111 (2007) 16951-16961.
[37] A.M. Beale, M.G. O'Brien, M. Kasunic, A. Golobic, M. Sanchez-Sanchez, A.J.W. Lobo, D.W. Lewis, D.S. Wragg, S. Nikitenko, W. Bras, B. M. Weckhuysen, J. Phys. Chem. C 115 (2011) 6331-6340.
[38] M.E. Davis, R.F. Lobo, Chem. Mater. 4 (1992) 756-768.
[39] S. Mintova, S. Mo, T. Bein, Chem. Mater. 10 (1998) 4030-4036.
[40] H. van Heyden, S. Mintova, T. Bein, J. Mater. Chem. 16 (2006) 514-518.

Table 1. Gel composition and experimental synthesis conditions of the different samples CoAPO-5 used in this article.

Sample	Gel composition (mol)[a]				Crystallization	
	w	*x*	*y*	*z*	time (h)	T (K)
CoAPO-5-TPA*	0.96	0.04	0.6 (TPA)	60	18	423
CoAPO-5-st	0.96	0.04	0.8	25	18	448
CoAPO-5-2h	0.96	0.04	0.8	25	2	448
CoAPO-5-4h	0.96	0.04	0.8	25	4	448
CoAPO-5-483K-2h	0.96	0.04	0.8	25	2	483
CoAPO-5-483K-18h	0.96	0.04	0.8	25	18	483
CoAPO-5-2%	0.98	0.02	0.8	25	18	448
CoAPO-5-8%	0.92	0.08	0.8	25	18	448
CoAPO-5-Cl	0.96	0.04	0.8	25	18	448
CoAPO-5-0.5MCHA	0.96	0.04	0.5	25	18	448
CoAPO-5-1.6MCHA	0.96	0.04	1.6	25	18	448
CoAPO-5-5H_2O	0.96	0.04	0.8	5	18	448
CoAPO-5-MW-1h	0.96	0.04	0.8	25	1	448
CoAPO-5-MW-1.5h	0.96	0.04	0.8	25	1.5	448
CoAPO-5-MW-4h	0.96	0.04	0.8	25	4	448

[a] *w*, *x*, *y* and *z* are the molar ratios according to the general gel composition: *w* Al : *x* Co : 1.0 P : *y* MCHA : *z* H_2O

Table 2. Some physical parameters of the samples CoAPO-5-2h, CoAPO-5-4h and CoAPO-5-st (18 h) estimated from XRD and N_2 isotherms data.

Sample	Crystal size[a] Sch, nm	Crystal width W-H, nm	Mesop. Surf. area[c], m^2/g	PSD max. (ads)[e], nm	PSD max. (des)[f], nm	Mesopor. Vol. ads.[g], cm^3/g
CoAPO-5-2h	40	48	81	19.4	9.4	0.106
CoAPO-5-4h	49	65	65	25.8	15.9	0.097
CoAPO-5-st	67	98	58	30.4	18	0.080

[a] Crystal size estimated by application of Scherrer equation according to the method described elsewhere [13].
[b] Crystal width as determined by Williansom-Hall plot, according to the method described elsewhere [13].
[c] Mesoporous surface area determined by subtracting microporous BET surface area from total BET surface area in calcined samples.
[e] Maximun of pore size distribution from adsorption branches, applying BJH method.
[f] Maximun of pore size distribution from adsorption branches, applying BJH method.
[g] Mesopore volume measured from adsorption branches.

Figure captions

Figure 1. Region of the XRD patterns in the 2θ range 19-23º of the samples CoAPO-5-st and CoAPO-5-TPA.

Figure 2. SEM images of the samples CoAPO-5-TPA (left) and CoAPO-5-st (right). An insert of a portion of a CoAPO-5-st particle is also shown. Note through the size-scaled bar the very different magnification used for the shown images, what gives an idea of the difference in particle/crystal size.

Figure 3. N_2 adsorption/desorption isotherms at 77 K of the calcined samples CoAPO-5-st and CoAPO-5-TPA. The adsorbed volume by micropores and mesopores is approximately indicated in the plot.

Figure 4. Region of the XRD patterns in the 2θ range 19-23º of the samples CoAPO-5-2h, CoAPO-5-4h and CoAPO-5-st.

Figure 5. N_2 adsorption/desorption isotherms at 77 K of both calcined and uncalcined samples CoAPO-5-2h, CoAPO-5-4h and CoAPO-5-st.

Figure 6. N_2 adsorption/desorption isotherms at 77 K of the samples uncalcined CoAPO-5-2h, CoAPO-5-st, CoAPO-5-483K-2h and CoAPO-5-st

Figure 7. SEM images of a representative crystal aggregate of the sample CoAPO-5-2%, CoAPO-5-st and CoAPO-5-8%. The approximate average diameter of the particles of each sample is indicated. Note through the size-scaled bar the very different magnification used for the shown images, what gives an idea of the difference in particle size.

Figure 8. N_2 adsorption/desorption isotherms at 77 K of the uncalcined samples $AlPO_4$-5, CoAPO-5-2%, CoAPO-5-st and CoAPO-5-8%.

Figure 9. Region of the XRD patterns in the 2θ range 19-23º of the samples CoAPO-5-st and CoAPO-5-0.5MCHA.

Figure 10. SEM images registered at different magnifications of a representative particle of the sample CoAPO-5-0.5MCHA.

Figure 11. N_2 adsorption/desorption isotherms at 77 K of the uncalcined samples CoAPO-5-st and CoAPO-5-0.5MCHA.

Figure 12. SEM images registered at different magnifications of the sample CoAPO-5-5H_2O.

Figure 13. N_2 adsorption/desorption isotherms at 77 K of the uncalcined samples CoAPO-5-st and CoAPO-5-5H_2O.

Figure 14. Region of the XRD patterns in the 2θ range 19.4-20.3º of the samples CoAPO-5-st, CoAPO-5-2h and the samples prepared under microwave-assisted hydrothermal treatment CoAPO-5-MW-1h, CoAPO-5-MW-1.5h and CoAPO-5-4h.

Figure 15. SEM images registered at different magnifications of the sample CoAPO-5-MW-1h.

Figure 16. N_2 adsorption/desorption isotherms at 77 K of the uncalcined samples CoAPO-5-2h, CoAPO-5-st, CoAPO-5-MW-1h and CoAPO-5-MW-4h.

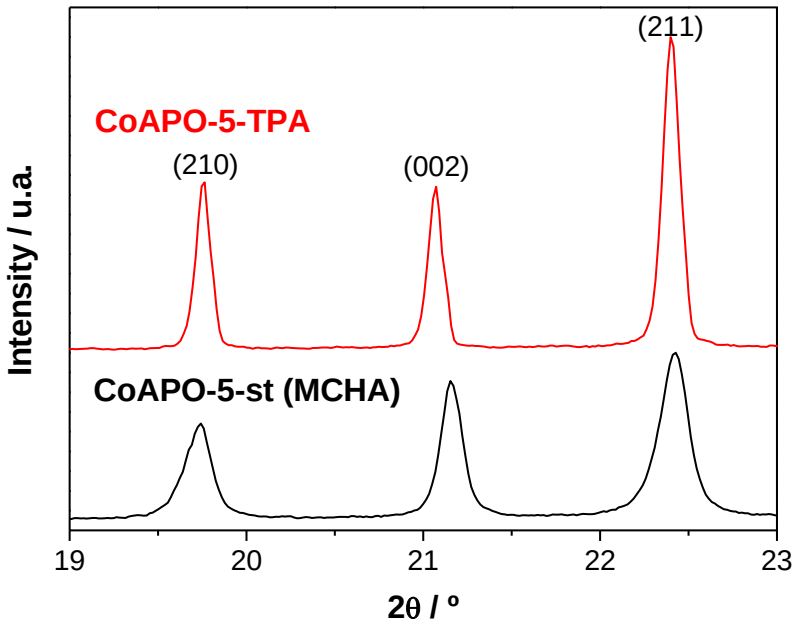
(211)
CoAPO-5-TPA
(210)
(002)
Intensity / u.a.
CoAPO-5-st (MCHA)
19
20
21
22
23
2θ / °

Figure 1

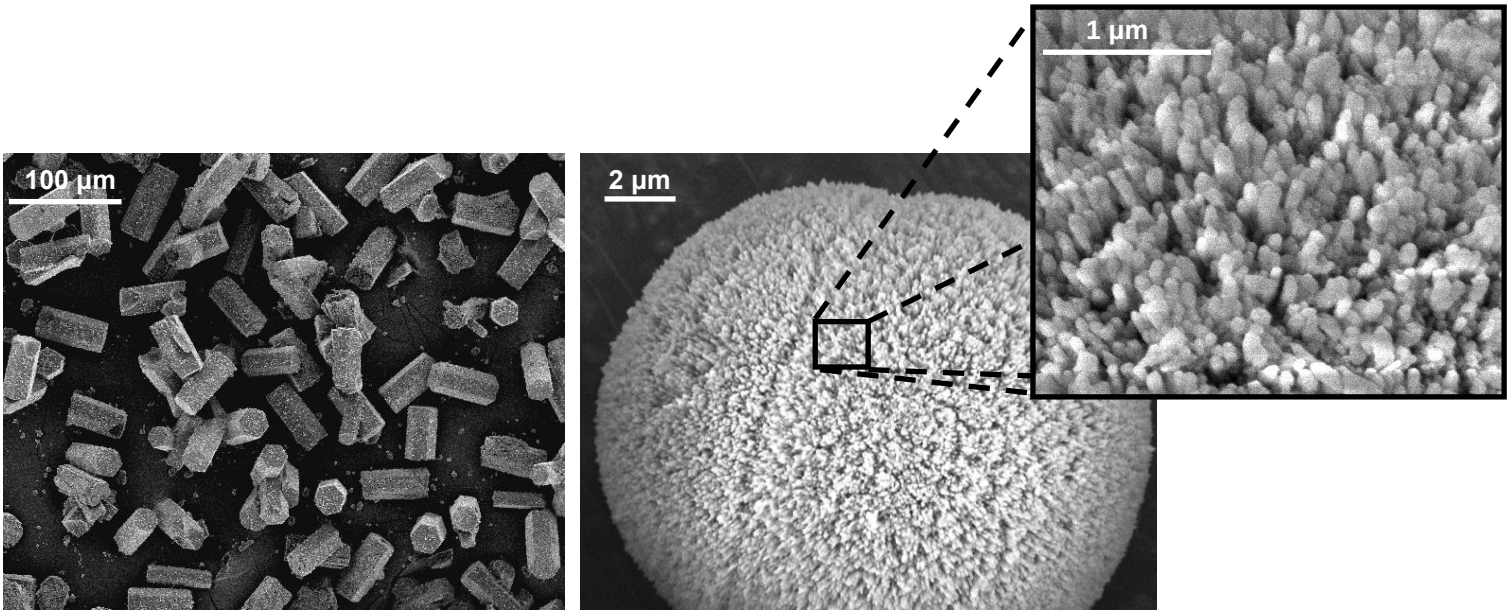

Figure 2

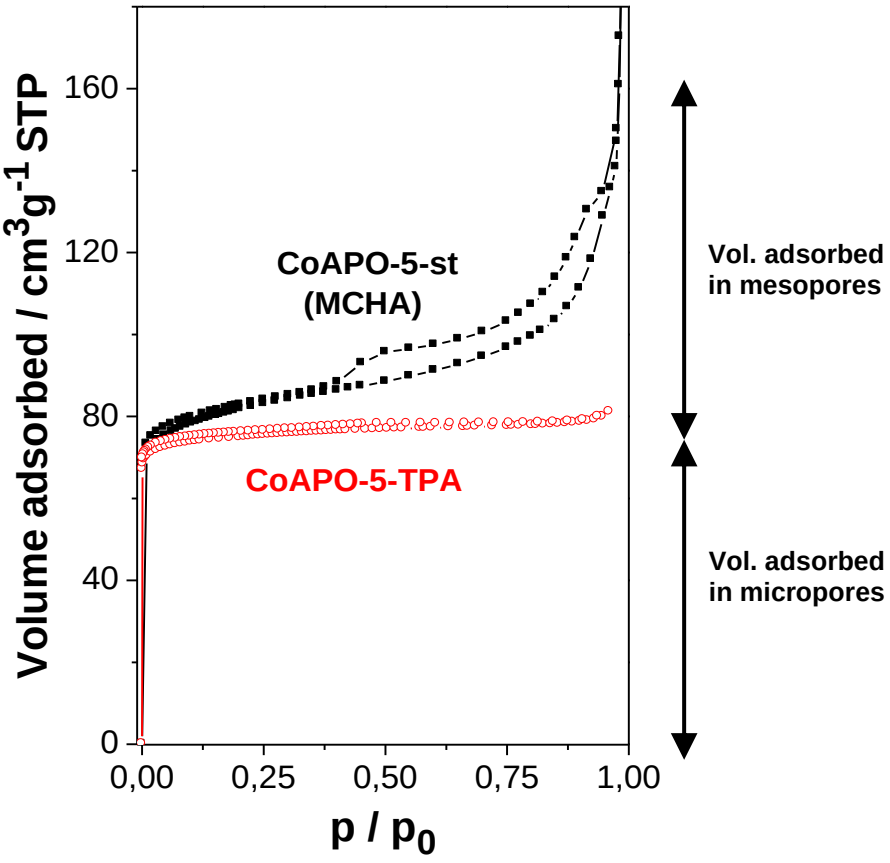
Volume adsorbed / cm3g-1 STP
160
120
80
40
0
0,00
0,25
0,50
0,75
1,00
p / p0
CoAPO-5-st
(MCHA)
CoAPO-5-TPA
Vol. adsorbed
in mesopores
Vol. adsorbed
in micropores

Figure 3

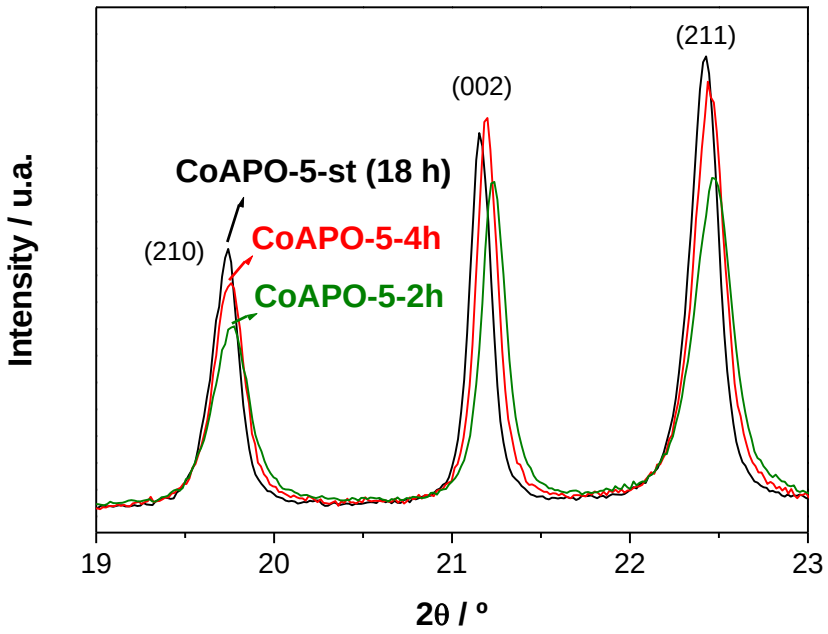
(211)
(002)
CoAPO-5-st (18 h)
(210)
CoAPO-5-4h
CoAPO-5-2h
Intensity / u.a.
19
20
21
22
23
2θ / °

Figure 4

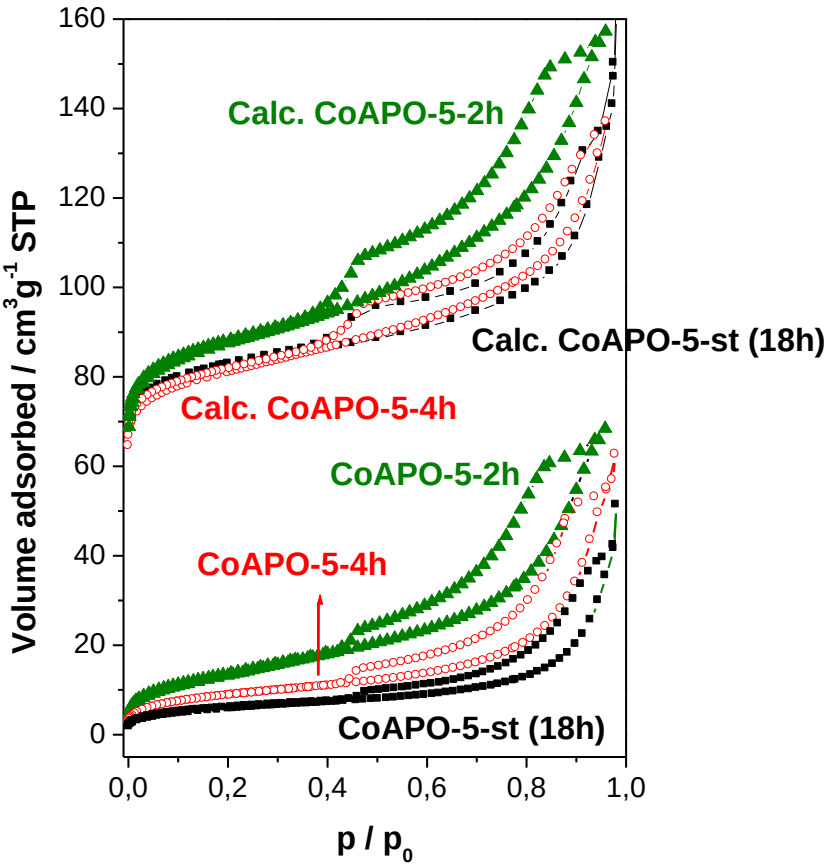
Calc. CoAPO-5-2h
Calc. CoAPO-5-st (18h)
Calc. CoAPO-5-4h
CoAPO-5-2h
CoAPO-5-4h
CoAPO-5-st (18h)
Volume adsorbed / cm3g-1 STP
p / p0
160
140
120
100
80
60
40
20
0
0,0
0,2
0,4
0,6
0,8
1,0

Figure 5

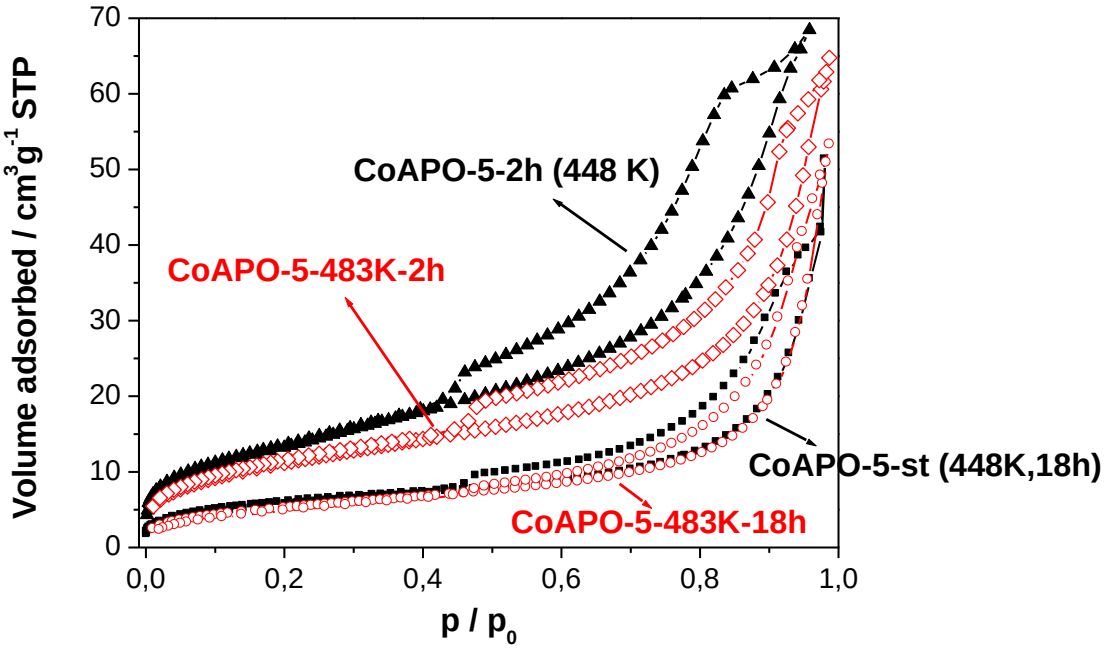
Volume adsorbed / cm3g-1 STP
p / p0
CoAPO-5-2h (448 K)
CoAPO-5-483K-2h
CoAPO-5-st (448K,18h)
CoAPO-5-483K-18h
0
10
20
30
40
50
60
70
0,0
0,2
0,4
0,6
0,8
1,0

Figure 6

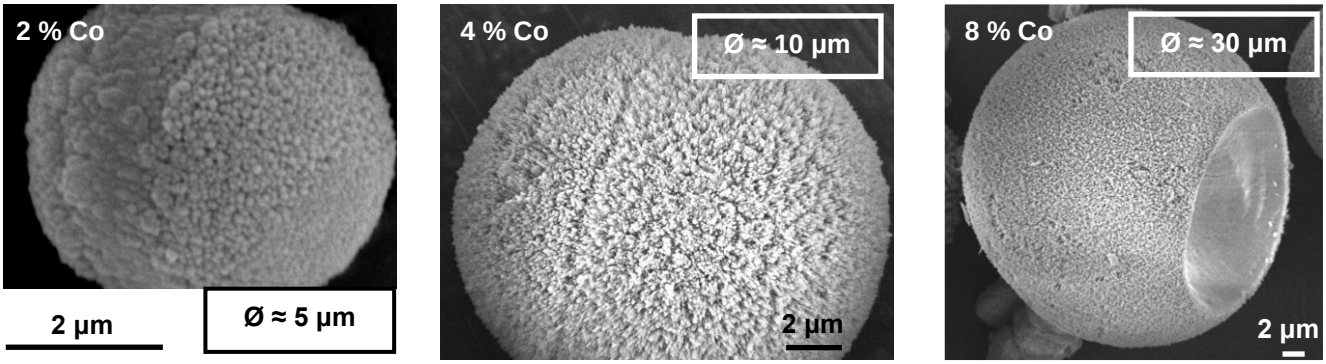

Figure 7

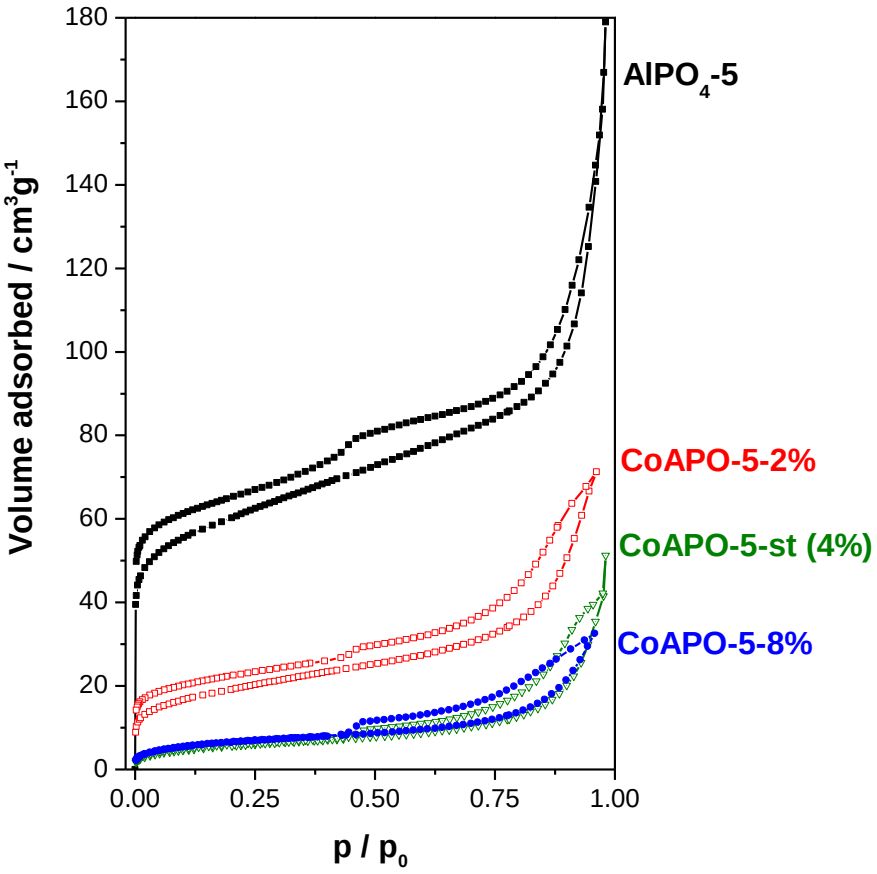
Volume adsorbed / cm3g-1
p / p0
AlPO4-5
CoAPO-5-2%
CoAPO-5-st (4%)
CoAPO-5-8%
0
20
40
60
80
100
120
140
160
180
0.00
0.25
0.50
0.75
1.00

Figure 8

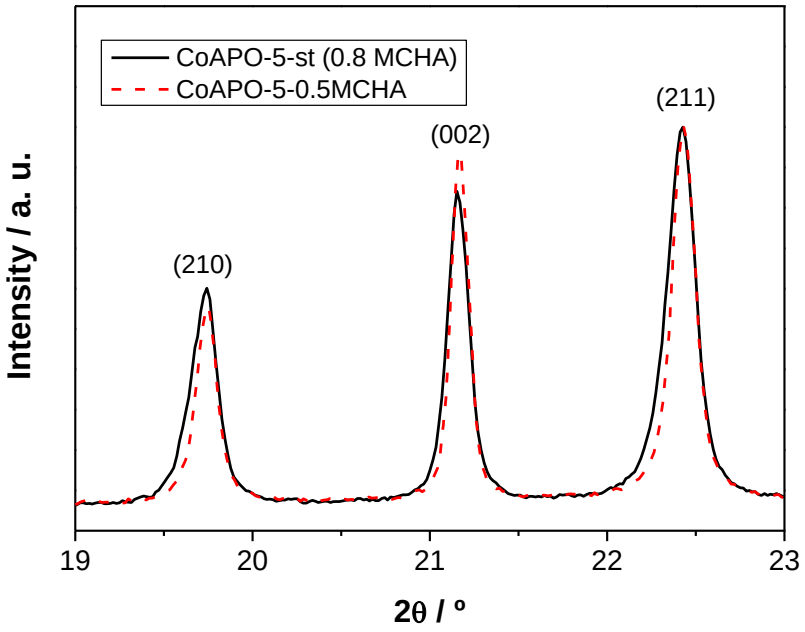
CoAPO-5-st (0.8 MCHA)
CoAPO-5-0.5MCHA
(210)
(002)
(211)
Intensity / a. u.
19
20
21
22
23
2θ / °

Figure 9

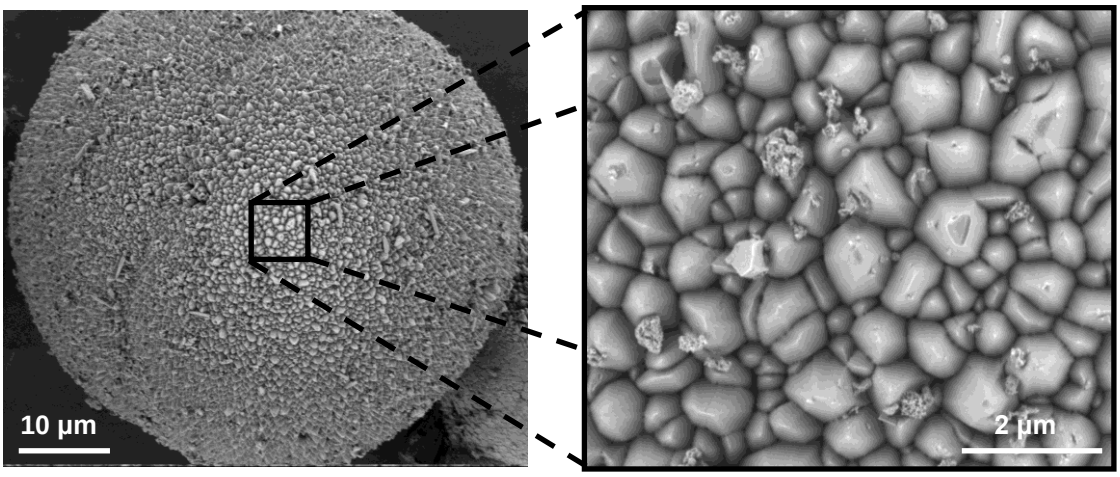

Figure 10

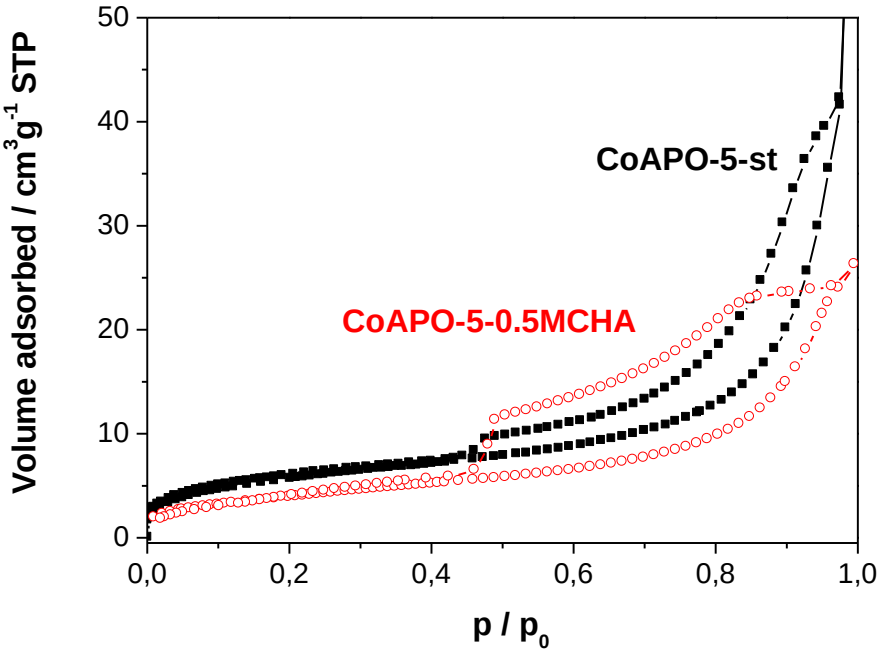
Volume adsorbed / cm3g-1 STP
p / p0
CoAPO-5-st
CoAPO-5-0.5MCHA
0
10
20
30
40
50
0,0
0,2
0,4
0,6
0,8
1,0

Figure 11

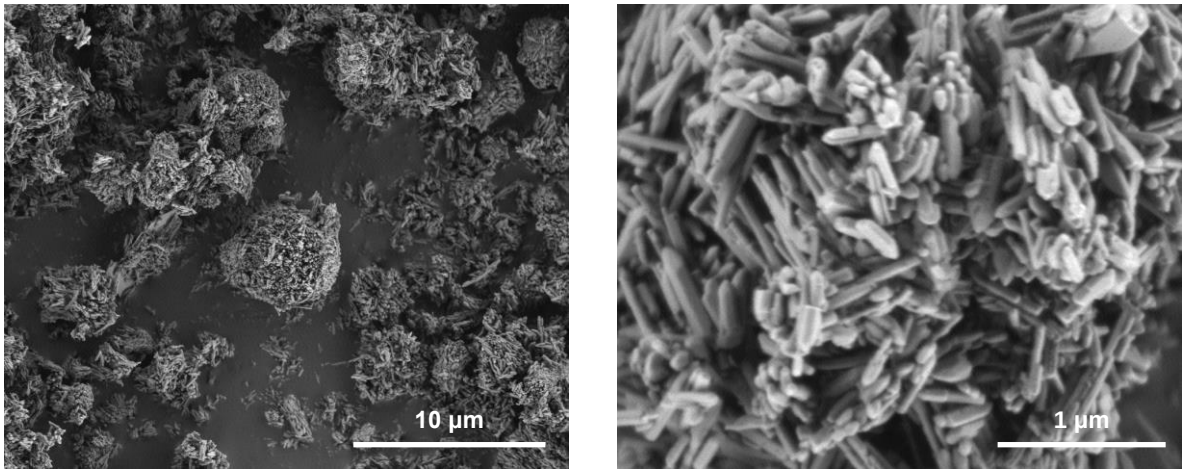

Figure 12

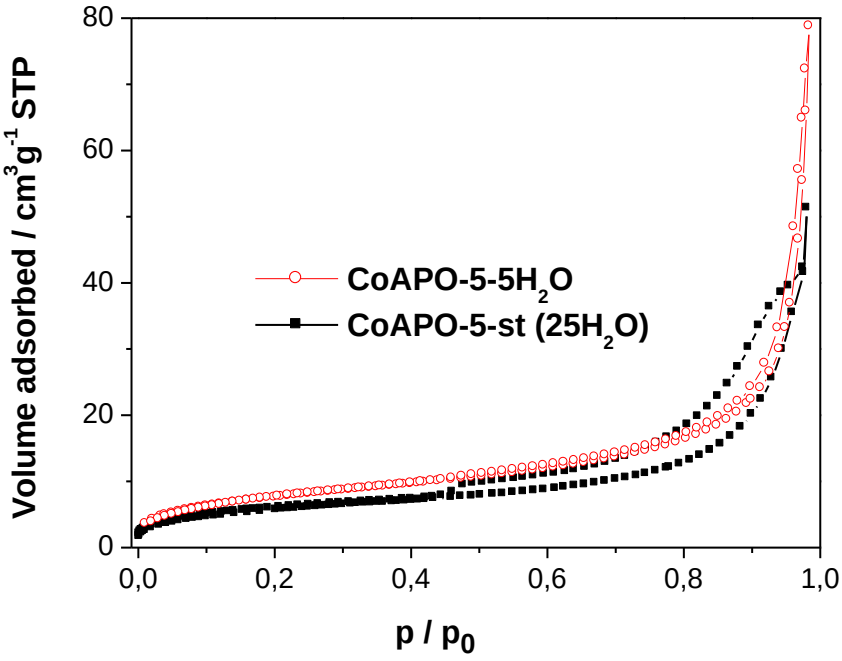
Volume adsorbed / cm3g-1 STP
80
60
40
20
0
0,0
0,2
0,4
0,6
0,8
1,0
p / p0
CoAPO-5-5H2O
CoAPO-5-st (25H2O)

Figure 13

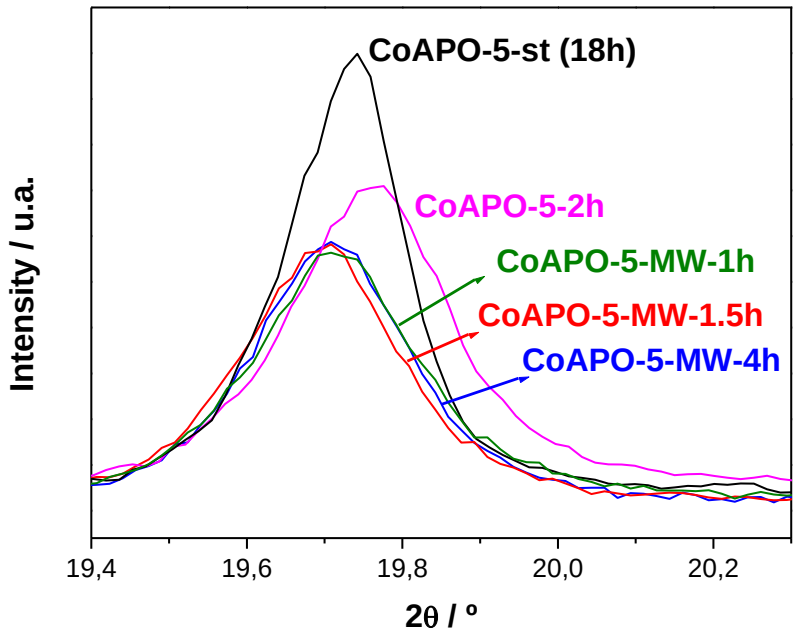
CoAPO-5-st (18h)
CoAPO-5-2h
CoAPO-5-MW-1h
CoAPO-5-MW-1.5h
CoAPO-5-MW-4h
Intensity / u.a.
19,4
19,6
19,8
20,0
20,2
2θ / °

Figure 14

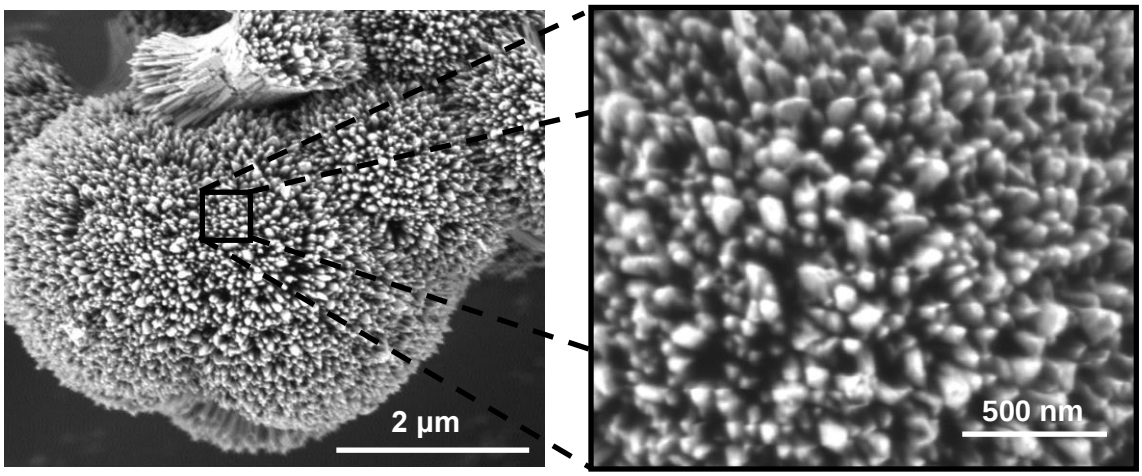

Figure 15

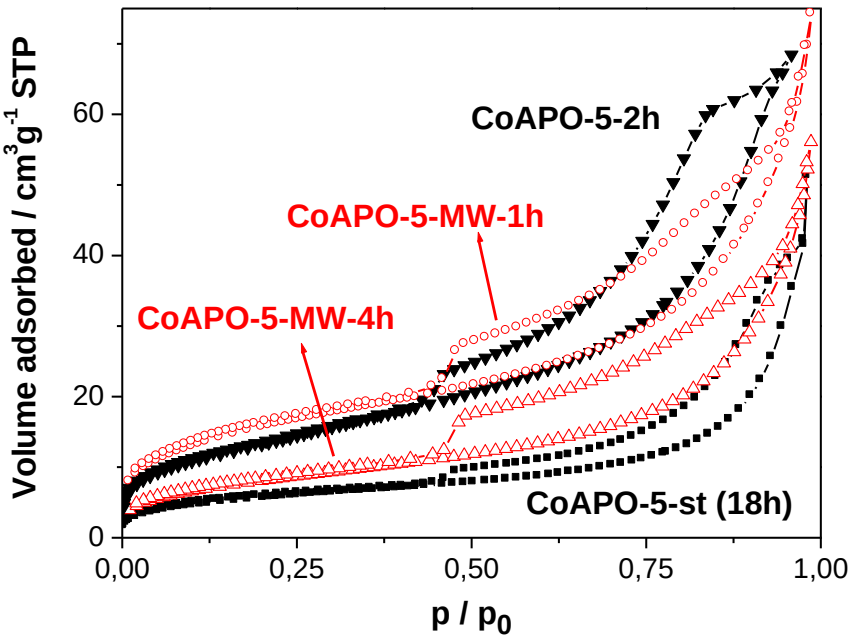
Volume adsorbed / cm3g-1 STP
60
40
20
0
0,00
0,25
0,50
0,75
1,00
p / p0
CoAPO-5-2h
CoAPO-5-MW-1h
CoAPO-5-MW-4h
CoAPO-5-st (18h)

Figure 16